

Band structure of phononic crystals with general damping

Mahmoud I. Hussein¹ and Michael J. Frazier¹

¹*Department of Aerospace Engineering Sciences, University of Colorado at Boulder, Boulder, Colorado 80309, USA**

In this chapter, we present theoretical formalisms for the study of wave dispersion in damped elastic periodic materials. We adopt the well-known structural dynamics techniques of modal analysis and state-space transformation and formulate them for the Bloch wave propagation problem. First, we consider a one-dimensional lumped parameter model of a phononic crystal whereby two masses connected by springs and viscous dashpot dampers compose the unit cell. We then extend our analysis to the study of a two-dimensional phononic crystal, modeled as a dissipative elastic continuum, and consisting of square inclusions periodically distributed within a host material. For our damping model, we consider both proportional damping and general damping. Our results demonstrate the effects of a range of damping levels on the frequency band structure for two distinct damping scenarios. In particular, we reveal two intriguing phenomena: branch overtaking and branch cut-off. The former may result in an abrupt drop in the relative band gap size, and the latter implies an opening of full or partial wavenumber (wave vector) band gaps. Following our frequency band structure analysis, we illustrate the concept of a damping ratio band structure.

I. INTRODUCTION

Phononic crystals are elastic materials whereby the microstructure geometry or constituent material phases are distributed periodically in space. With careful size scaling and choice of the constituent material phases and their spatial distribution within the periodic unit cell, phononic crystals can be designed to classically control the propagation of acoustic/elastic waves in a predetermined manner. In doing so, these modern materials have opened up a technological frontier in acoustic and elastic devices [1–3]. Bloch theory [4] provides the underlying mathematical framework for obtaining the fundamental wave propagation characteristics in phononic crystals. Through this theory, it is possible to obtain a relationship between frequency and wavenumber (wave vector) — this relationship is referred to as the frequency band structure. In many cases, one or more of the constituent materials are damped (i.e., dissipative), a good example is viscoelastic materials which are often used to form the matrix phase in phononic crystal composites. The presence of damping results in temporal and spatial attenuations of the elastic waves as they freely “progress” through the periodic media [5]. It is therefore necessary to establish rigorous theoretical formalisms for damped Bloch wave propagation, which is the objective of this chapter.

To follow is a brief survey of various studies in the literature that dealt with damping in infinite (and finite) periodic materials (and structures). In an early study focusing on one-dimensional (1D) discrete mass-spring-dashpot models, Mead [5] considered structural (velocity independent) damping as well as a hypothetical type of damping associated with what was referred to as “damped forced modes”. Viscous damping was treated later on with various types of dissipative con-

stitutive models. Mukherjee and Lee [6], for example, provided a dispersion relation using a complex elastic modulus to model viscoelasticity in a 1D laminated medium. Tassilly [7] on the other hand considered viscous damping which was mathematically incorporated in the governing equations as a *separate* term representing velocity-dependent damping forces. He analyzed 1D periodic beam structures suspended on an elastic foundation, which is a unique configuration that produces no acoustical branches in the frequency spectrum. In other studies, often the focus has been on finite structures or there was little consideration of the broad effects on the band structure characteristics (e.g., Refs. [8–10]). Some studies explicitly investigated the band structure using viscoelastic damping models, although limited to a fixed frequency [11, 12] or to low frequencies [13]. Wang *et al.* [14] analytically studied dispersion in 1D viscoelastic lattices with a model applicable to a wide frequency range. Merheb *et al.* [15] also provided a study that was not limited to certain frequencies, using the finite difference time-domain method in addition to experiments. Yet both these studies did not provide a detailed analysis of the broad effects of damping on the dispersion band structure. In Ref. [15], the conclusions were focused on the spatial attenuation/decay effects. Recently, Lee *et al.* [16] proposed a method whereby effective medium theory is employed in conjunction with the transfer matrix method to analyze 1D damped periodically layered materials.

In Refs. [17] and [18], the concept of *Bloch modal analysis* has been introduced for the study of the dynamics of periodic media. The concept was first employed for the purpose of model reduction for band structure calculations [17], and was later utilized for the study of the effects of proportional (Rayleigh) damping on the band structure and phase and group velocity dispersion relations [18]. In this chapter, we further utilize Bloch modal analysis towards investigating the effects of both stiffness- and mass-proportional damping on the dispersion relation. Our primary objective, however, is to

* Corresponding author email: mih@colorado.edu

broaden our treatment of damped periodic media by developing a theoretical formalism, based on state-space transformation, for the study of systems with general damping. For both the proportional damping and general damping problems, we consider 1D and two-dimensional (2D) viscously damped phononic crystal models and explicitly show the effects of damping on the frequency versus wavenumber wave vector curves. In doing so, we highlight two intriguing phenomena — *branch overtaking* and *branch cut-off*. In branch overtaking the presence of damping causes the higher branches in the band structure to drop in frequency at rates that exceed the drop rates for lower branches, thus causing the overtake. Branch cut-off refers to a state whereby a dispersion branch does not cover the entire first Brillouin zone, thus creating a full or a partial band gap with respect to the wavenumber (wave vector) as opposed to the frequency. Finally we correlate our frequency band structure analysis with the corresponding representation of the damping ratio-wavenumber (wave vector) relations, i.e., *damping ratio band structure*.

In this work, we consider constant damping parameters in our treatment of viscous damping. However, since we assume harmonic motion in time, the viscous dissipation force, \mathbf{f}_{vd} is frequency-dependent, i.e., $\mathbf{f}_{\text{vd}} = \hat{\mathbf{C}}\dot{\mathbf{u}} = \lambda(\omega)\hat{\mathbf{C}}\mathbf{u}$, where \mathbf{u} denotes the displacement vector, $\hat{\mathbf{C}}$ denotes the damping matrix, $\lambda(\omega)$ denotes a frequency-dependent coefficient, ω denotes frequency, and the dot symbolizes differentiation with respect to time. This is in contrast, for example, to what is known as structural damping which generates a frequency-independent force $\mathbf{f}_{\text{sd}} = i\mu\hat{\mathbf{K}}\mathbf{u}$, where $\hat{\mathbf{K}}$ denotes the stiffness matrix, μ is a damping parameter, and $i = \sqrt{-1}$. Reference to the frequency-dependence of damping is often made to the damping matrix itself as opposed to the damping forces. Incorporating frequency-dependence in the $\hat{\mathbf{C}}$ matrix, i.e., $\hat{\mathbf{C}} = \hat{\mathbf{C}}(\omega)$, is a subject for future research.

The layout of the chapter consists of two parts: Sec. II covers a discrete model and Sec. III covers a continuous model. In each section, we present the theory and subsequently provide numerical examples for both proportional and general damping.

II. DISCRETE MODEL

II.1. Theory

We begin our study of damped periodic materials by considering a simple 1D lumped parameter lattice model which we use to demonstrate the basic characteristics of dispersive behavior due to damping. Our system, which is by definition infinite in extent, is constructed by appending copies of the two-mass unit cell of Fig. 1 along the line of motion. The lattice spacing is denoted by a .

The set of equations that describe the motion of the

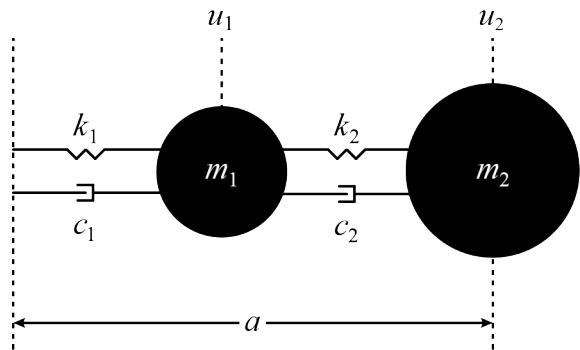


FIG. 1. Discrete model of phononic crystal: two-mass unit cell.

two masses, m_1 and m_2 , in the unit cell are

$$m_1\ddot{u}_1^j + (c_1 + c_2)\dot{u}_1^j + (k_1 + k_2)u_1^j - c_2\dot{u}_2^j - k_2u_2^j - c_1\dot{u}_2^{j-1} - k_1u_2^{j-1} = 0, \quad (1a)$$

$$m_2\ddot{u}_2^j + (c_1 + c_2)\dot{u}_2^j + (k_1 + k_2)u_2^j - c_2\dot{u}_1^j - k_2u_1^j - c_1\dot{u}_1^{j+1} - k_1u_1^{j+1} = 0, \quad (1b)$$

where u_ℓ^j represents the displacement of mass ℓ in the j th unit cell.

We assume a plane wave solution

$$u_\ell^j(x, \kappa, t) = \tilde{u}_\ell e^{i\kappa x + \lambda t}, \quad (2)$$

for mass ℓ at the j th lattice point, where \tilde{u}_ℓ , κ , x , and t denote the complex wave amplitude, wavenumber, position, and time, respectively. It should be noted that x is not continuous, reflecting the discreteness of the material model. Moreover, because the unit cell resides at each lattice point, the wave may only be sampled at those points, i.e., $x = \{-ja, \dots, -a, 0, a, \dots, ja\}$ (j is an integer). Due to the periodicity of the solution, the following statement holds for the displacement of mass ℓ at neighboring lattice points.

$$u_\ell^{j+n}(x + na, \kappa, t) = u_\ell^j(x, \kappa, t)e^{in\kappa a}, \quad (3)$$

In Eq. (3), the integer $n = 0$ for the present unit cell, $n = 1$ for the subsequent unit cell, and $n = -1$ for the previous unit cell. Substituting Eq. (3) into Eqs. (1a) and (1b) yields two homogeneous equations for u_1 and u_2 , respectively, i.e., in matrix form

$$\hat{\mathbf{M}}\ddot{\mathbf{u}} + \hat{\mathbf{C}}\dot{\mathbf{u}} + \hat{\mathbf{K}}\mathbf{u} = \mathbf{0}, \quad (4)$$

where $\hat{\mathbf{M}}$ denotes the mass matrix and $\mathbf{u} = [u_1 \ u_2]^T$ [$(\cdot)^T$ denotes the transpose operation]. The $\hat{\mathbf{M}}$, $\hat{\mathbf{C}}$, and $\hat{\mathbf{K}}$ matrices are explicitly defined as follows:

$$\hat{\mathbf{M}} = \begin{bmatrix} m_1 & 0 \\ 0 & m_2 \end{bmatrix},$$

$$\hat{\mathbf{C}} = \begin{bmatrix} c_1 + c_2 & -(e^{-i\kappa a}c_1 + c_2) \\ -(e^{i\kappa a}c_1 + c_2) & c_1 + c_2 \end{bmatrix},$$

$$\hat{\mathbf{K}} = \begin{bmatrix} k_1 + k_2 & -(e^{-i\kappa a}k_1 + k_2) \\ -(e^{i\kappa a}k_1 + k_2) & k_1 + k_2 \end{bmatrix}.$$

Applying the time derivatives, Eq. (4) becomes

$$(\lambda^2 \hat{\mathbf{M}} + \lambda \hat{\mathbf{C}} + \hat{\mathbf{K}})\mathbf{u} = \mathbf{0}, \quad (5)$$

$$\omega_s(\kappa) = \sqrt{\frac{(k_1 + k_2)(m_1 + m_2) \mp \sqrt{[(k_1 + k_2)(m_1 + m_2)]^2 - 8(1 - \cos \kappa a)k_1 k_2 m_1 m_2}}{2m_1 m_2}}, \quad s = 1, 2$$

where s refers to the mode number, which in the context of a dispersion band structure is the branch number.

II.1.1. General damping

For the case of general damping (where the damping matrix $\hat{\mathbf{C}}$ is nonzero, Hermitian, but nonproportional to $\hat{\mathbf{M}}$ or $\hat{\mathbf{K}}$) it is not possible to set up a Bloch eigenvalue problem in the usual way because of the presence of the viscous damping term. We therefore resort to converting the second-order problem to a first-order problem through a state-space transformation [19, 20]

$$\hat{\mathbf{A}}\hat{\mathbf{y}} + \hat{\mathbf{B}}\hat{\mathbf{y}} = \mathbf{0}, \quad (6)$$

where

$$\hat{\mathbf{A}} = \begin{bmatrix} \mathbf{0} & \hat{\mathbf{M}} \\ \hat{\mathbf{M}} & \hat{\mathbf{C}} \end{bmatrix}, \quad \hat{\mathbf{B}} = \text{diag}[-\hat{\mathbf{M}} \ \hat{\mathbf{K}}], \quad \hat{\mathbf{y}} = [\dot{\mathbf{u}} \ \mathbf{u}]^T.$$

For convenience, we define $r_m = m_2/m_1$, $r_c = c_2/c_1$, $r_k = k_2/k_1$, and subsequently write the $\hat{\mathbf{M}}$, $\hat{\mathbf{C}}$, and $\hat{\mathbf{K}}$ matrices in terms of only m_2 , c_2 , and k_2 respectively,

$$\begin{aligned} \hat{\mathbf{M}} &= m_2 \hat{\mathbf{M}}_o = m_2 \begin{bmatrix} 1/r_m & 0 \\ 0 & 1 \end{bmatrix}, \\ \hat{\mathbf{C}} &= c_2 \hat{\mathbf{C}}_o = c_2 \begin{bmatrix} 1 + 1/r_c & -(e^{-i\kappa a}/r_c + 1) \\ -(e^{i\kappa a}/r_c + 1) & 1 + 1/r_c \end{bmatrix}, \\ \hat{\mathbf{K}} &= k_2 \hat{\mathbf{K}}_o = k_2 \begin{bmatrix} 1 + 1/r_k & -(e^{-i\kappa a}/r_k + 1) \\ -(e^{i\kappa a}/r_k + 1) & 1 + 1/r_k \end{bmatrix}. \end{aligned}$$

Utilizing this notation and dividing by m_2 , the state-space matrices $\hat{\mathbf{A}}$ and $\hat{\mathbf{B}}$ become

$$\hat{\mathbf{A}} = \begin{bmatrix} \mathbf{0} & \hat{\mathbf{M}}_o \\ \hat{\mathbf{M}}_o & \beta \hat{\mathbf{C}}_o \end{bmatrix}, \quad \hat{\mathbf{B}} = \text{diag}[-\hat{\mathbf{M}}_o \ \omega_0^2 \hat{\mathbf{K}}_o],$$

where $\omega_0 = \sqrt{k_2/m_2}$ and $\beta = c_2/m_2$. We assume a solution for Eq. (6) of the form $\hat{\mathbf{y}} = \bar{\mathbf{y}}e^{\gamma t}$. The damped frequency band structure can now be obtained by solving the associated eigenvalue problem. The eigenvalues, which appear in complex conjugate pairs, are solutions to the characteristic equation

$$\gamma^4 + a\gamma^3 + b\gamma^2 + c\gamma + d = 0,$$

For $\hat{\mathbf{C}} = \mathbf{0}$, the familiar eigenvalue problem emerges. With eigenvalue $\lambda^2 = -\omega^2$, the dispersion relation is easily obtained. In the case of the phononic crystal represented by the unit cell in Fig. 1, the undamped frequency-wavenumber relation is

with

$$\begin{aligned} a &= \frac{(1 + r_c)(1 + r_m)\beta}{r_c}, \\ b &= \frac{2(1 - \cos \kappa a)r_k r_m \beta^2 + (1 + r_k)(1 + r_m)r_c \omega_0^2}{r_c r_k}, \\ c &= \frac{2(1 - \cos \kappa a)(r_c + r_k)r_m \beta \omega_0^2}{r_c r_k}, \\ d &= \frac{2r_m \omega_0^4 (1 - \cos \kappa a)}{r_k}. \end{aligned}$$

The form of the solution resembles that from structural dynamics, except, in the context of Bloch wave propagation, the terms are dependent upon the wavenumber (wave vector).

$$\gamma(\kappa) = -\xi_s(\kappa)\omega_s(\kappa) \pm i\omega_{d,s}(\kappa), \quad s = 1, 2 \quad (7)$$

In Eq. (7), the real part is the negative of the product of the wavenumber-dependent damping ratio, $\xi_s(\kappa)$, and the resonant frequency, $\omega_s(\kappa)$; the imaginary part is the wavenumber-dependent frequency of damped wave propagation $\omega_{d,s}(\kappa)$ for mode s . Corresponding to each eigenvalue, the frequency of damped free wave propagation and the associated damping ratio are simply

$$\begin{aligned} \omega_{d,s}(\kappa) &= \text{Im}[\gamma_s(\kappa)], \quad s = 1, 2 \\ \xi_s(\kappa) &= -\frac{\text{Re}[\gamma_s(\kappa)]}{\text{Abs}[\gamma_s(\kappa)]}, \quad s = 1, 2. \end{aligned}$$

Since each member of a conjugate pair describes the same wave with only the direction of propagation in opposition, no information is lost in considering only the member with $\text{Im}[\gamma_s(\kappa)] > 0$.

II.1.2. Proportional (Rayleigh) damping

The advantage of the state-space formulation is its applicability to a generalized viscous damping matrix; however, the size of the eigenvalue problem doubles. For the special case of Rayleigh damping (see Ref. [21] for a discussion on the limitations of this model), $\hat{\mathbf{C}}$ is linearly proportional to $\hat{\mathbf{M}}$ and/or $\hat{\mathbf{K}}$, i.e.,

$$\hat{\mathbf{C}} = p\hat{\mathbf{M}} + q\hat{\mathbf{K}} \quad (8)$$

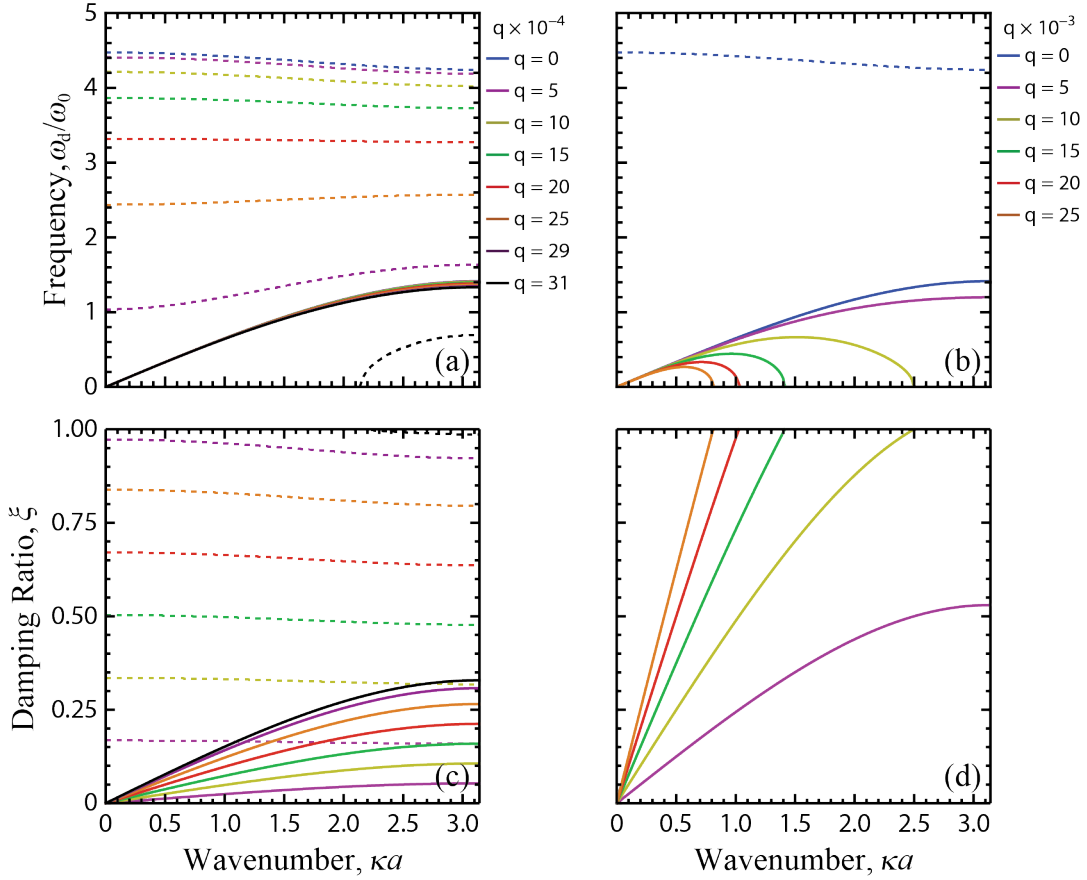


FIG. 2. Stiffness-proportional damping dispersion curves and damping ratio band diagrams.

where $p, q \geq 0$ are scaling parameters. Naturally, $p, q = 0$ corresponds to the undamped case. In circumstances of proportional damping, the size of the problem need not be doubled through a state-space transformation. Instead, we can now employ the concept of Bloch modal analysis [18] which allows us to linearly transform the model degrees of freedom \mathbf{u} to a set of Bloch generalized degrees of freedom, \mathbf{v} , that is, $\mathbf{u} = \mathbf{\Phi}\mathbf{v}$. Unlike in Ref. [17] in which the aim is model reduction, here the matrix $\mathbf{\Phi}$ is formed using a set of mass-normalized Bloch vectors obtained by solving the standard undamped eigenvalue problem at the current κ point.

Substituting Eq. (8) into Eq. (5) yields

$$[\lambda^2 \hat{\mathbf{M}} + \lambda(p\hat{\mathbf{M}} + q\hat{\mathbf{K}}) + \hat{\mathbf{K}}]\mathbf{u} = \mathbf{0}. \quad (9)$$

Utilizing the orthogonality condition that the Bloch vectors exhibit with respect to $\hat{\mathbf{M}}$ and $\hat{\mathbf{K}}$, the expansion uncouples the equations in Eq. (9). This is done by substituting $\mathbf{u}(t) = \mathbf{\Phi}\mathbf{v}(t)$ into Eq. (9) and pre-multiplying by $\mathbf{\Phi}^H$ [$(\cdot)^H$ denotes the Hermitian transpose operation]

$$\mathbf{\Phi}^H[\lambda^2 \hat{\mathbf{M}} + \lambda(p\hat{\mathbf{M}} + q\hat{\mathbf{K}}) + \hat{\mathbf{K}}]\mathbf{\Phi}\mathbf{v} = \mathbf{0}. \quad (10)$$

Equation (10) simplifies to

$$[\lambda^2 \mathbf{I} + \lambda(p\mathbf{I} + q\mathbf{\Lambda}) + \mathbf{\Lambda}]\mathbf{v} = \mathbf{0}, \quad (11)$$

where $\mathbf{\Lambda}$ is a diagonal matrix of eigenvalues. Equation (11) represents two uncoupled equations expressed in matrix form. Analogous to the treatment of single degree-of-freedom finite systems in structural dynamics, each of these equations can be written in terms of the damping ratio $\xi_s(\kappa)$ and the undamped frequency $\omega_s(\kappa)$,

$$[\lambda_s^2 + 2\xi_s(\kappa)\omega_s(\kappa)\lambda + \omega_s^2(\kappa)]v_s = 0, \quad s = 1, 2. \quad (12)$$

Comparing Eqs. (11) and (12) gives

$$2\xi_s(\kappa)\omega_s(\kappa) = p + q\omega_s^2(\kappa). \quad (13)$$

From Eq. (13), the damping ratio is derived explicitly

$$\xi_s(\kappa) = \frac{1}{2} \left[\frac{p}{\omega_s(\kappa)} + q\omega_s(\kappa) \right], \quad s = 1, 2.$$

Solving for the roots of Eq. (12), we get

$$\lambda_s(\kappa) = -\xi_s(\kappa)\omega_s(\kappa) \pm \omega_s(\kappa)\sqrt{\xi_s^2(\kappa) - 1}, \quad s = 1, 2 \quad (14)$$

which, for the underdamped case, $[\xi_s(\kappa) < 1]$ is by definition equal to

$$\lambda_s(\kappa) = -\xi_s(\kappa)\omega_s(\kappa) \pm i\omega_{d,s}(\kappa), \quad s = 1, 2.$$

Hence, the wavenumber-dependent frequency of damped

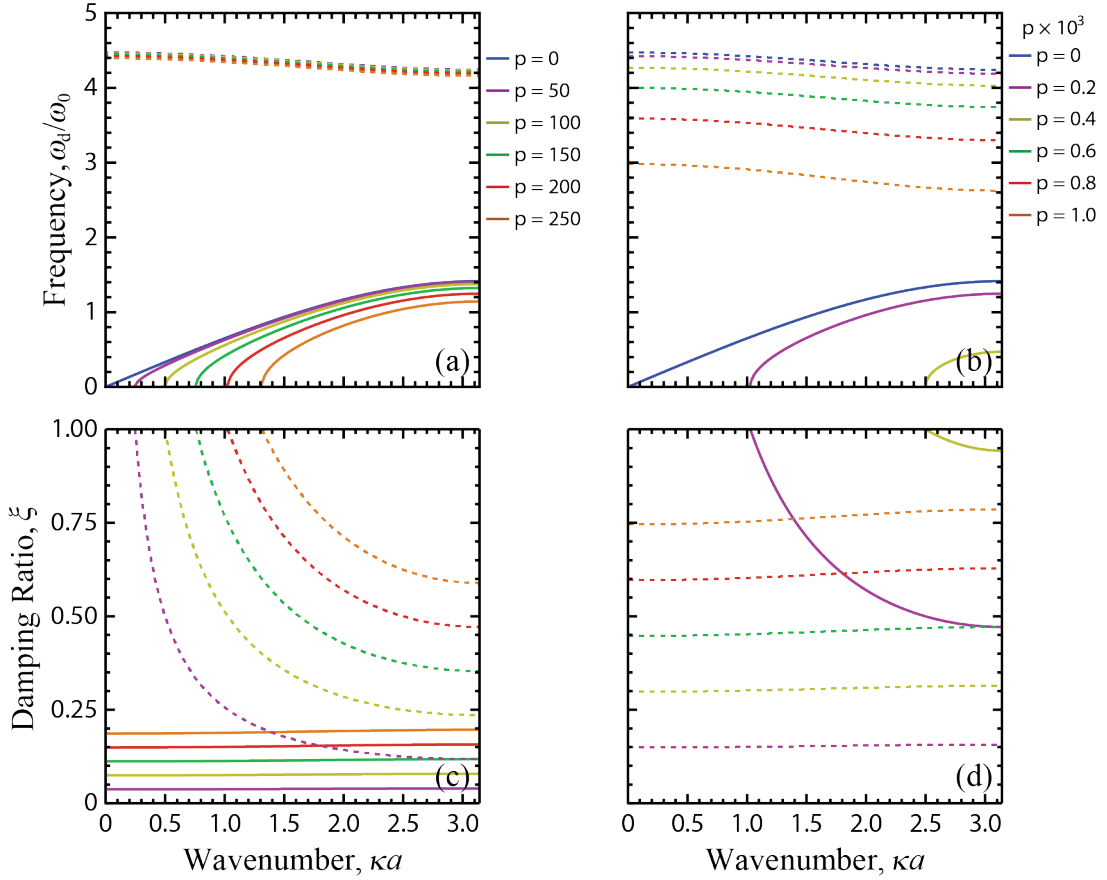


FIG. 3. Mass-proportional damping dispersion curves and damping ratio band diagrams.

wave propagation is

$$\begin{aligned} \omega_{d,s}(\kappa) &= \omega_s(\kappa) \sqrt{1 - \xi_s^2(\kappa)} \\ &= \omega_s(\kappa) \sqrt{1 - \frac{1}{4} \left[\frac{p}{\omega_s(\kappa)} + q\omega_s(\kappa) \right]^2}, \quad s = 1, 2. \end{aligned}$$

For the undamped case [$\xi_s(\kappa) = 0$], the frequency of the s th branch of the original undamped band structure [i.e., $\omega_s(\kappa)$] is recovered. For $\xi_s(\kappa) > 1$, the medium is overdamped and temporal oscillations do not exist. The medium is critically damped when $\xi_s(\kappa) = 1$. It is noteworthy that this theory is analogous to the well-established modal analysis (modal decomposition) theory for proportionally damped finite structures [19, 20].

II.2. Results

To examine our formulation, we select a specific set of material constants for our two-mass model as follows: $r_m = 9$, $r_c = 1/2$, $r_k = 1$, and $\omega_0 = \sqrt{k_2/m_2} = 150 \text{ rad/s}$.

II.2.1. Effects of different types of damping

We consider three different damping cases – stiffness-proportional, mass-proportional, and general damping – and, for each case, present both the frequency band structure and the damping ratio band structure for various levels of damping intensity. In all the figures concerned with this two-mass system, the frequency of the acoustical branch, $\omega_{d,1}$, is represented by a solid curve, while the frequency of the optical branch, $\omega_{d,2}$, is represented by a dashed curve. In addition, the undamped curves are always colored blue and the damped curves are colored otherwise.

In Fig. 2, we show the results for the stiffness-proportional damping case (i.e., $p = 0$ and $q > 0$). It is apparent from Fig. 2a that the optical frequency branch is more affected by the damping than the acoustical frequency branch; indeed, as most apparent in Fig. 2c, the optical branch's corresponding value of damping ratio increases more rapidly than that of the acoustical branch. As the level of damping increases, the curve for $\omega_{d,2}/\omega_0$ flattens out and eventually transitions from being concave down to concave up before vanishing. The downward concavity of $\omega_{d,1}/\omega_0$ remains the same, but, as shown in Fig. 2b, the range of κa over which $\omega_{d,1}/\omega_0 > 0$

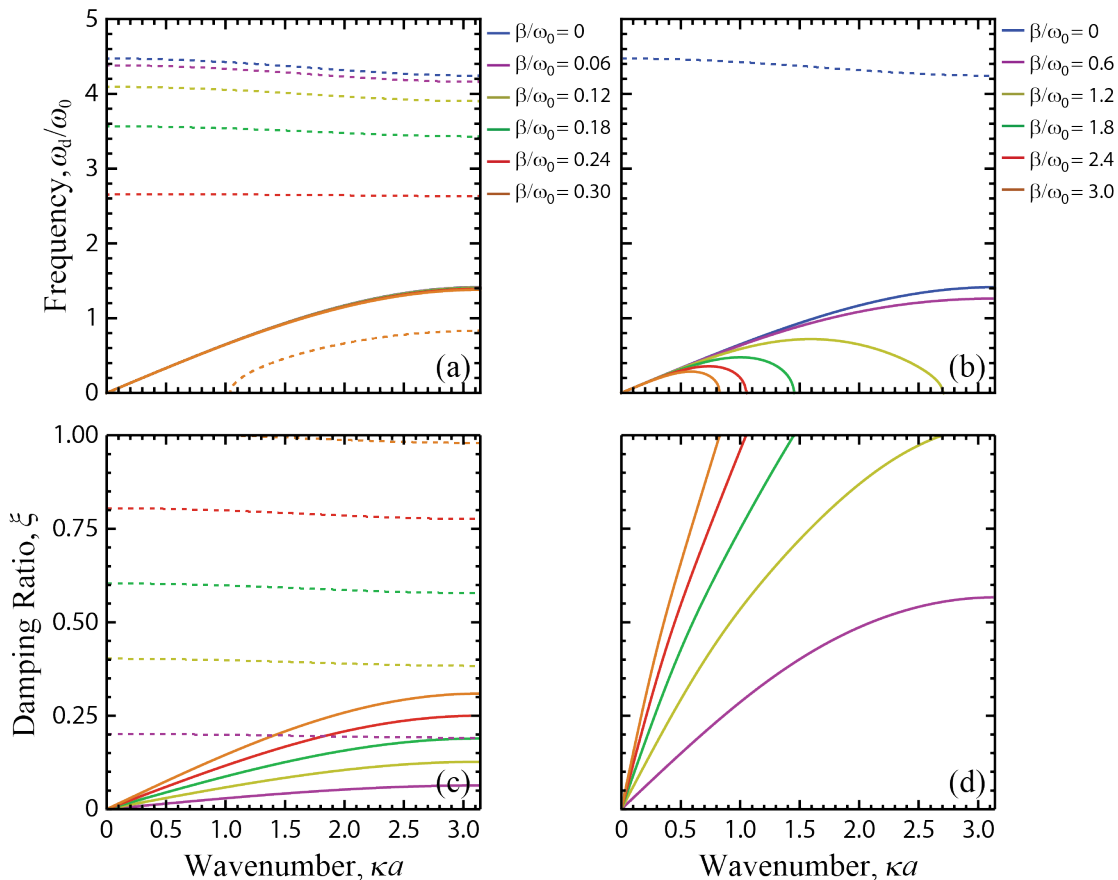


FIG. 4. General damping dispersion curves.

decreases as the damping intensifies.

The results for mass-proportional damping (i.e., $p > 0$ and $q = 0$) are shown in Fig. 3. Comparing Fig. 3a with Fig. 2a, it is clear that mass-proportional damping has the opposite effect on the acoustical and optical frequency branches than that induced by stiffness-proportional damping. The acoustical frequency branch is affected more by this type of damping and accordingly the corresponding damping ratio values increase more rapidly. Unlike in Fig. 2a, the concavity of both curves remains constant while, like in Fig. 2a, the range of κa over which propagation is possible ($\omega_{d,1}/\omega_0 > 0$) decreases. In this case, low-frequency waves possessing longer wavelengths ($\kappa a \rightarrow 0$) are the first to become overdamped.

Emerging from the state-space transformation approach, Fig. 4 presents the frequency band structure for a general damping model for various values of β/ω_0 . A comparison of Figs. 2 and 4 reveals a similarity in the dispersive effects of stiffness-proportional damping and the present condition of general damping. These similarities in the dispersion band structure can be explained by the mathematical similarities between the $\hat{\mathbf{K}}$ matrix and the $\hat{\mathbf{C}}$ matrix due to the common placement of springs and viscous dampers in Fig. 1. $\hat{\mathbf{C}}$ and $q\hat{\mathbf{K}}$ are structurally

similar being full matrices, while $\hat{\mathbf{C}}$ and the diagonal $p\hat{\mathbf{M}}$ are structurally dissimilar. As for stiffness-proportional damping, in Fig. 4, $\omega_{d,2}$ is more susceptible to the influences of damping than is $\omega_{d,1}$. The optical frequency branch flattens out before changing concavity (not shown in Fig. 4).

It is noteworthy that the band structure alterations described above induce both quantitative and qualitative changes to the group velocity dispersion curves. For example, it is possible for the group velocity of some branches to switch from positive to negative as a result of damping [18].

II.2.2. Branch overtaking and branch cut-off

In the results presented for the damped mass-spring periodic chain, we can observe two intriguing phenomena that emerge due to the presence of damping: *branch overtaking* and *branch cut-off*. Branch overtaking takes place when higher branches in the band structure drop in frequency at rates that exceed the drop rates for lower branches, thus causing the overtake. A branch cut-off refers to a state whereby a dispersion branch does not cover the entire first Brillouin zone, thus creating a par-

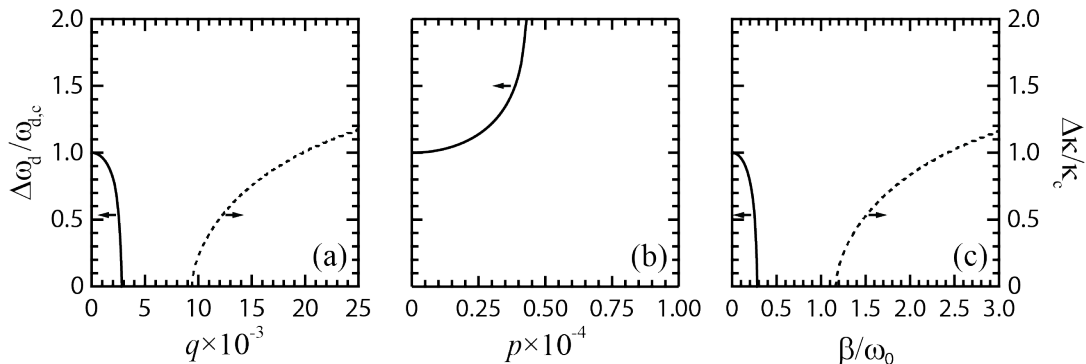


FIG. 5. Frequency (solid lines) and wavenumber (dashed lines) band gaps as a function of damping level for the (a) stiffness-proportional, (b) mass-proportional, and (c) general damping cases considered.

tial band gap with respect to the wavenumber (or wave vector for a multi-dimensional problem) as opposed to the frequency.

In Figs. 2a and 4a, we observe cases of branch overtaking. In particular, we observe in each case that the location of the optical branch shifts down the frequency domain at a much faster rate than the acoustical branch as the intensity of damping is increased. For example, in Fig. 4a the optical branch is located below the acoustical branch when $\beta/\omega_0 = 0.3$. Damping and the higher drop rate of the optical branch causes the band gap to decrease in size at an increasing rate. This is quantitatively illustrated by tracking the relative size of the band gap with respect to its central frequency as a function of damping intensity, as illustrated in Fig. 5. Clearly the relative band gap size rate drops for the stiffness-proportional and general damping cases. For the mass-proportional damping situation, a greater rate of descent for the acoustical branch compared to the optical results in an increasing band gap and, therefore, no branch over-taking. In some cases (as reported in Ref. [18]), if the overtake takes place on an optical branch, a band gap can drop in size even more abruptly.

In Figs. 2b, 3a, and 4b, we observe another damping-induced phenomenon in the frequency band structure. We observe, that when the level of damping exceeds a certain value, the acoustical branch gets cut off in the wavenumber domain, i.e., it does not span the entire first Brillouin zone. Moreover, since the optical branch eventually disappears in the cases of Figs. 2a and 4b (due to the presence of a high level of damping), we get a *wavenumber band gap*, i.e., a wavenumber range where waves are prohibited from propagation. This phenomenon is clearly analogous to the well-known concept of a frequency band gap. In the case presented in Fig. 3a, we observe a partial wavenumber band gap as the optical branch remains. In Fig. 5, we track the opening of the relative width of the wavenumber band gap for the three damping cases studied.

The damping-induced branch-overtaking and branch cut-off phenomena clearly present opportunities for de-

sign, building on already existing methodologies at the unit cell level [22, 23] and/or at the combination of the unit cell and structural levels [24].

III. CONTINUOUS MODEL

III.1. Theory

In this section, we consider a continuous phononic crystal governed by

$$\nabla \cdot \boldsymbol{\sigma} = \rho \ddot{\mathbf{u}}, \quad (15)$$

where $\boldsymbol{\sigma}$ is the stress tensor, ρ is the density, and $\mathbf{u} = \{u_x, u_y, u_z\}$ is now used to denote the displacement field. The constitutive behavior is treated phenomenologically assuming linear and isotropic elastic response and viscous damping,

$$\boldsymbol{\sigma} = \mathbf{C}_K : \nabla^S \mathbf{u} + \mathbf{C}_C : \nabla^S \dot{\mathbf{u}}, \quad (16)$$

where \mathbf{C}_K is the conventional elasticity tensor, \mathbf{C}_C is the viscous damping tensor, and ∇^S denotes the symmetric gradient operator, that is,

$$\nabla^S \mathbf{u} = \frac{1}{2} [\nabla \mathbf{u} + (\nabla \mathbf{u})^T]. \quad (17)$$

Substituting Eq. (16) into Eq. (15) yields

$$\nabla \cdot \mathbf{C}_K : \nabla^S \mathbf{u} + \nabla \cdot \mathbf{C}_C : \nabla^S \dot{\mathbf{u}} = \rho \ddot{\mathbf{u}}. \quad (18)$$

We will assume that the unit cell is composed of two or more material phases, and that the material-to-material interfaces are ideal. Equation (18) has a Bloch solution of the form

$$\mathbf{u}(\mathbf{x}, \boldsymbol{\kappa}, t) = \tilde{\mathbf{u}}(\mathbf{x}) e^{i\boldsymbol{\kappa} \cdot \mathbf{x} + \lambda t}, \quad (19)$$

where $\tilde{\mathbf{u}}(\mathbf{x})$ is the periodic displacement Bloch amplitude function with the periodicity of the medium, \mathbf{x} is the position vector, and $\boldsymbol{\kappa}$ is the wave vector. Similar to

discrete counterpart in Eq. (2), periodicity enforces the following identity

$$\mathbf{u}(\mathbf{x} + \mathbf{a}, \boldsymbol{\kappa}, t) = \mathbf{u}(\mathbf{x}, \boldsymbol{\kappa}, t)e^{i\boldsymbol{\kappa} \cdot \mathbf{a}}.$$

Using Eq. (19), the spatial component of the displacement gradient is

$$\nabla \mathbf{u} = (\nabla \tilde{\mathbf{u}} + i\boldsymbol{\kappa} \otimes \tilde{\mathbf{u}})e^{i\boldsymbol{\kappa} \cdot \mathbf{x}}, \quad (20)$$

where the symbol \otimes denotes the outer product. Similarly, the velocity gradient is

$$\nabla \dot{\mathbf{u}} = (\nabla \dot{\tilde{\mathbf{u}}} + i\boldsymbol{\kappa} \otimes \dot{\tilde{\mathbf{u}}})e^{i\boldsymbol{\kappa} \cdot \mathbf{x}}. \quad (21)$$

Substitution of Eqs. (17), (19), (20), and (21) into Eq. (18) gives the strong form of the Bloch eigenvalue problem

$$\begin{aligned} \nabla \cdot \mathbf{C}_K : \left[\nabla^S \tilde{\mathbf{u}} + \frac{i}{2}(\boldsymbol{\kappa} \otimes \tilde{\mathbf{u}} + \tilde{\mathbf{u}} \otimes \boldsymbol{\kappa}) \right] \\ + \nabla \cdot \mathbf{C}_C : \left[\nabla^S \dot{\tilde{\mathbf{u}}} + \frac{i}{2}(\boldsymbol{\kappa} \otimes \dot{\tilde{\mathbf{u}}} + \dot{\tilde{\mathbf{u}}} \otimes \boldsymbol{\kappa}) \right] = \rho \ddot{\tilde{\mathbf{u}}}. \end{aligned} \quad (22)$$

Applying the time derivatives, Eq. (22) becomes

$$\begin{aligned} \nabla \cdot \mathbf{C}_K : \left[\nabla^S \tilde{\mathbf{u}} + \frac{i}{2}(\boldsymbol{\kappa} \otimes \tilde{\mathbf{u}} + \tilde{\mathbf{u}} \otimes \boldsymbol{\kappa}) \right] \\ + \gamma \nabla \cdot \mathbf{C}_C : \left[\nabla^S \dot{\tilde{\mathbf{u}}} + \frac{i}{2}(\boldsymbol{\kappa} \otimes \dot{\tilde{\mathbf{u}}} + \dot{\tilde{\mathbf{u}}} \otimes \boldsymbol{\kappa}) \right] = \gamma^2 \rho \tilde{\mathbf{u}}. \end{aligned} \quad (23)$$

Equation (23) can be discretized using a numerical method. We will consider the finite element (FE) method [17], but it should be noticed that the following treatment of damping is independent of the specific choice the numerical method. The discretization transforms the continuous Bloch displacement functions to discrete Bloch displacement vectors, yielding

$$\hat{\mathbf{M}}\ddot{\tilde{\mathbf{u}}} + \hat{\mathbf{C}}\dot{\tilde{\mathbf{u}}} + \hat{\mathbf{K}}\tilde{\mathbf{u}} = \mathbf{0}, \quad (24)$$

and

$$[\gamma^2 \hat{\mathbf{M}} + \gamma \hat{\mathbf{C}} + \hat{\mathbf{K}}]\tilde{\mathbf{u}} = \mathbf{0}, \quad (25)$$

respectively. $\hat{\mathbf{M}}$, $\hat{\mathbf{C}}$, and $\hat{\mathbf{K}}$ now denote the finite element mass, damping, and stiffness matrices. In Eqs. (24) and (25), the vectors are of size $n_e \times 1$ and each of the matrices is of size $n_e \times n_e$ where n_e denotes the number of FE equations.

For the undamped case, where $\hat{\mathbf{C}} = \mathbf{0}$, we realize that $\gamma = i\omega$ (hence $\mathbf{u}(\mathbf{x}; t) = \tilde{\mathbf{u}}(\mathbf{x})e^{i\omega t}$) and subsequently obtain the familiar eigenvalue problem for undamped Bloch wave propagation

$$[\hat{\mathbf{K}} - \omega^2 \hat{\mathbf{M}}]\tilde{\mathbf{u}} = \mathbf{0}.$$

On the other hand, if the second term in the left-hand-side of Eq. (25) is nonzero, this prevents us from generating an eigenvalue problem in the usual way for calculating the band structure.

III.1.1. General damping

To enable a formal eigenvalue analysis of a problem exhibiting general damping, we transform Eq. (24) into the state-space formulation consistent with Eq. (6). In this case, the eigenvalue solution is wave vector-dependent:

$$\lambda_s(\boldsymbol{\kappa}) = -\xi_s(\boldsymbol{\kappa})\omega_s(\boldsymbol{\kappa}) \pm i\omega_{d,s}(\boldsymbol{\kappa}), \quad s = 1, \dots, n_e. \quad (26)$$

In the same manner as in the discrete case, we can extract $\xi_s(\boldsymbol{\kappa})$ and $\omega_{d,s}(\boldsymbol{\kappa})$ from Eq. (26).

III.1.2. Proportional (Rayleigh) damping

As discussed earlier in Sec. II.1.2, a special case for a phononic crystal damping model is proportional damping [18]. We will define the proportional viscous finite element matrix similarly as given in Eq. (8), substitute into Eq. (24), and subsequently obtain

$$\hat{\mathbf{M}}\ddot{\tilde{\mathbf{u}}} + [p\hat{\mathbf{M}} + q\hat{\mathbf{K}}]\dot{\tilde{\mathbf{u}}} + \hat{\mathbf{K}}\tilde{\mathbf{u}} = \mathbf{0}. \quad (27)$$

As we did in the discrete case, we employ the concept of Bloch mode expansion [17, 18] which allows us to linearly transform the model to a set of Bloch generalized coordinates, $\tilde{\mathbf{v}}^T(t) = [\tilde{v}_1(t) \ \tilde{v}_2(t) \ \dots \ \tilde{v}_m(t)]$, i.e.,

$$\tilde{\mathbf{u}}(t)_{(n_e \times 1)} = \boldsymbol{\Phi}_{(n_e \times m)} \tilde{\mathbf{v}}_{(m \times 1)}(t), \quad (28)$$

where $\boldsymbol{\Phi}$ is a Bloch modal matrix. In Eq. (28), m denotes the total number of Bloch modes retained in the expansion. We follow the same procedure as in Sec. II.1.2, and utilize the orthogonality condition that the Bloch vectors exhibit with respect to $\hat{\mathbf{M}}$ and $\hat{\mathbf{K}}$ at the current $\boldsymbol{\kappa}$ -point to uncouple the governing equations. This is done by substituting Eq. (28) into Eq. (27) and pre-multiplying all terms by $\boldsymbol{\Phi}^H$. Returning to Eq. (28), only as many Bloch modes m need to be incorporated in the expansion as the number of branches of interest in the damped band diagram that is to be generated. The result is a set of m uncoupled equations

$$\ddot{\tilde{v}}_s + 2\xi_s(\boldsymbol{\kappa})\omega_s(\boldsymbol{\kappa})\dot{\tilde{v}}_s + [\omega_s(\boldsymbol{\kappa})]^2\tilde{v}_s = 0, \quad s = 1, \dots, m. \quad (29)$$

where \tilde{v}_s is the s th Bloch generalized coordinate and $\omega_s(\boldsymbol{\kappa})$ represents the wavenumber-dependent frequency of undamped wave propagation (as in the discrete case). In Eq. (29), $\xi_s(\boldsymbol{\kappa})$ is the damping ratio of the s th branch (out of a total of m branches) of the damped band structure at point $\boldsymbol{\kappa}$ and is defined as

$$\xi_s(\boldsymbol{\kappa}) = \frac{1}{2} \left[\frac{p}{\omega_s(\boldsymbol{\kappa})} + q\omega_s(\boldsymbol{\kappa}) \right], \quad s = 1, \dots, m. \quad (30)$$

Applying the derivatives in Eq. (29) and solving for the roots yields a similar expression as given in Eq. (14)

$$\lambda_s(\boldsymbol{\kappa}) = -\xi_s(\boldsymbol{\kappa})\omega_s(\boldsymbol{\kappa}) \pm \omega_s(\boldsymbol{\kappa})\sqrt{\xi_s^2(\boldsymbol{\kappa}) - 1}, \quad s = 1, \dots, m.$$

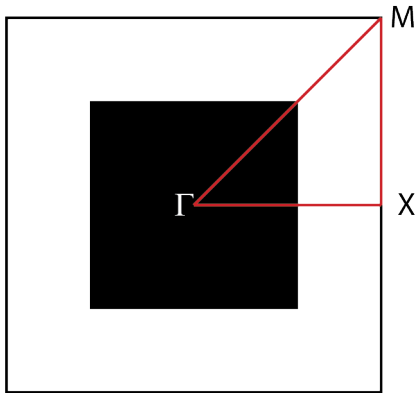


FIG. 6. Continuous model of phononic crystal with irreducible Brillouin zone enclosed in red.

For the undamped case [$\xi_s(\boldsymbol{\kappa}) = 0$], the frequency of the s th branch of the original undamped band structure is recovered. For $\xi_s(\boldsymbol{\kappa}) < 1$, the medium is underdamped at $\boldsymbol{\kappa}$ and propagating waves exhibit temporal decay in time. Subsequently,

$$\lambda_s(\boldsymbol{\kappa}) = -\xi_s(\boldsymbol{\kappa})\omega_s(\boldsymbol{\kappa}) \pm i\omega_{d,s}(\boldsymbol{\kappa}), \quad s = 1, \dots, m$$

and the wave vector-dependent frequency of damped oscillation is defined as

$$\omega_{d,s}(\boldsymbol{\kappa}) = \omega_s(\boldsymbol{\kappa})\sqrt{1 - \xi_s^2(\boldsymbol{\kappa})}, \quad s = 1, \dots, m \quad (31)$$

which is essentially the frequency of the s th branch of the damped band structure at point $\boldsymbol{\kappa}$. For $\xi_s(\boldsymbol{\kappa}) > 1$, the medium is overdamped at $\boldsymbol{\kappa}$ and temporal oscillations cannot exist. The medium is critically damped at $\boldsymbol{\kappa}$ when $\xi_s(\boldsymbol{\kappa}) = 1$.

III.2. Results

In this section, we examine the behavior of a continuous model of both a proportionally damped and a generally damped phononic crystal. We use the finite element method to discretize the spatial domain in both cases. For the proportionally damped case we solve Eq. (29) and proceed to calculating $\xi_s(\boldsymbol{\kappa})$ and $\omega_{d,s}(\boldsymbol{\kappa})$ by simply post-processing the resulting undamped band structure data using Eqs. (30) and (31), respectively. For the generally damped case we use the state-space formulation, solve for $\lambda_s(\boldsymbol{\kappa})$, and extract $\xi_s(\boldsymbol{\kappa})$ and $\omega_{d,s}(\boldsymbol{\kappa})$. Both damping-type formulations are applicable to three-dimensional models. However, for ease of exposition we present results for a 2D model under plane strain conditions. In our example model, a square lattice is considered with a bi-material unit cell consisting of a centrally located square inclusion, as shown in Fig. 6. The filling ratio is 0.3086. The material phase for the matrix (denoted by subscript “1”) is chosen to be compliant and light while the phase for the inclusion (denoted by subscript “2”) is stiff and dense. In particular, a ratio of

Young’s moduli of $E_2/E_1 = 20$ and a ratio of densities of $\rho_2/\rho_1 = 2$ are chosen. A Poisson ratio of $\nu = 0.34$ is assumed for both phases. The unit cell finite element mesh consists of 9×9 uniformly sized four-node bi-linear quadrilateral elements. The path along the symmetry points, $\Gamma \rightarrow X \rightarrow M \rightarrow \Gamma$, bordering the irreducible Brillouin zone is sampled into ninety-seven $\boldsymbol{\kappa}$ -point steps. In the results, we refer to the degree of proportional damping using the scaling parameters p and q . The shear Lamé constant for material phase “1” is denoted μ_1 . For the general damping case we perturb a stiffness-proportional damping model by multiplying each of the Lamé constants by a different scalar, thus breaking the proportionality of the damping matrix to the stiffness matrix.

Figure 7a,b shows the frequency band structure (restricted to real wave vectors) for the undamped case, where $p, q = 0$, a proportionally damped case with parameters $p = 0$ and $q = 0.05$, and a generally damped case whereby a proportionally damped model with parameters $p_{\text{scaled}} = 0$ and $q_{\text{scaled}} = 0.05$ is perturbed by replacing μ by $\mu_{\text{damp}} = 1.4\mu$ and λ by $\lambda_{\text{damp}} = 0.6\lambda$ in the damping matrix \mathbf{C} . The damping ratio corresponding to each mode, as a function of $\boldsymbol{\kappa}$, is shown in Fig. 7c,d. We observe that for the proportionally damped case considered the location of the branches in the frequency domain drop with damping, and do so at an increasing rate as the branch number increases. The damping ratio diagram shown in Fig. 7c resembles the frequency band structure in shape. Furthermore, the locations of the curves in Fig. 7a drop, and in Fig. 7c rise, with increase in the value of q (not shown). We also studied the case where $p \neq 0$ and $q = 0$ (not shown). Here, the band structure away from the Γ -point experiences very small shifts, whereas at and near the Γ -point the downward shift in frequencies is dramatic, and this is due to sharp increases in ξ_s within this neighborhood. In fact, with a small increase in p , the value of the damping ratio at and near the Γ -point exceeds unity, i.e., exceeds the critical damping level beyond which there is no temporal oscillations. We therefore focus on a nonzero q while keeping $p = 0$. The response of the considered generally damped case follows a similar trend to the proportionally damped case with deviations in certain regions such as between the M - and Γ -points, especially for the sixth branch. The damping ratio diagram for both cases also differ considerably especially at the high branches. Even though λ_{damp} was decreased at the same rate (40%) as μ_{damp} was increased in the general damping matrix, we observe that the level of overall damping in the band structure has increased compared to the nominal stiffness-proportionally damped case. This suggests that damping in shear has a more significant effect on the band structure than longitudinal damping. This conclusion is confirmed by considering the opposite case where μ has been replaced by $\mu_{\text{damp}} = 0.6\mu$ and λ by $\lambda_{\text{damp}} = 1.4\lambda$, the results of which are presented in Fig. 7b and d.

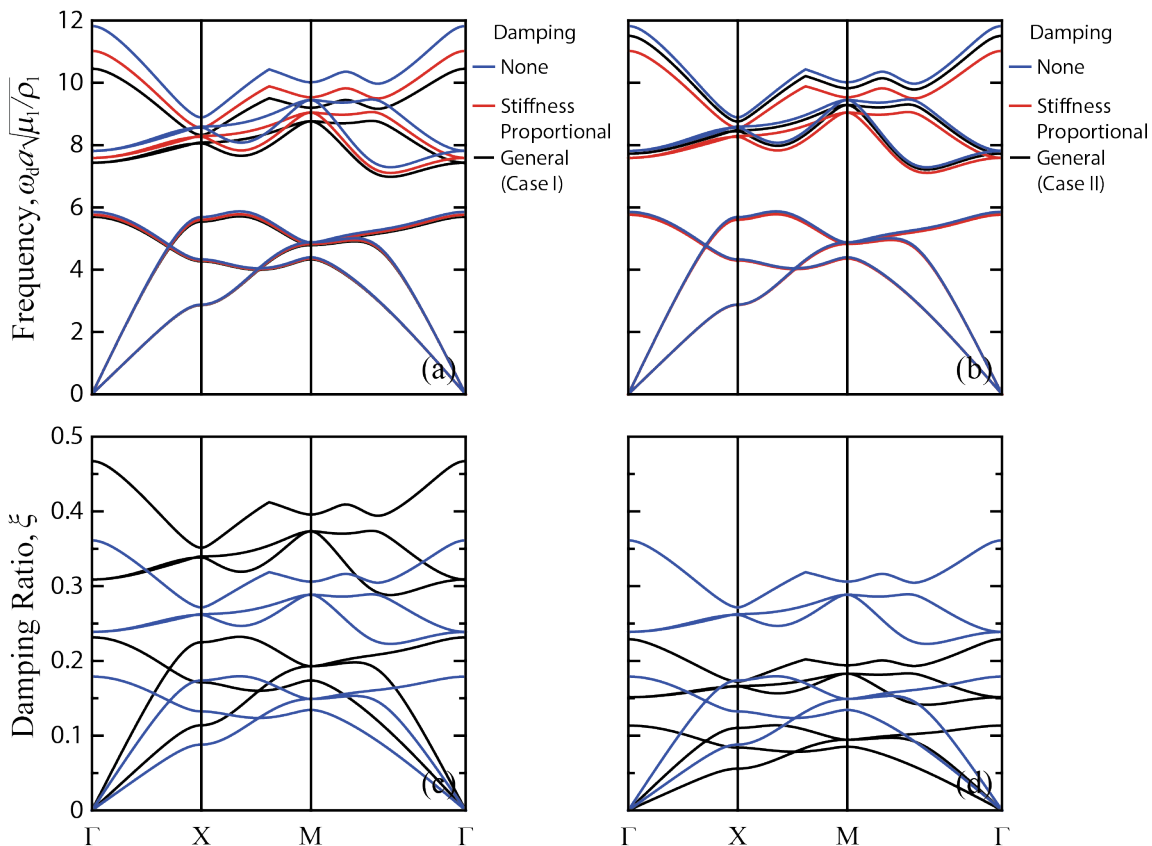


FIG. 7. Frequency (a,b) and damping ratio (c,d) band structures for.

IV. CONCLUSIONS

We presented a formal treatment of the Bloch wave propagation problem for viscously damped phononic crystals. We first studied an infinite chain consisting of two masses in the unit cell, then generalized to a continuum model of a phononic crystal which was subsequently discretized using the finite element method. We considered both the general damping case and the special case where the damping matrix is proportional to the mass and/or stiffness matrices. In all our analyses we presented the mathematical formulations governing the application of Bloch theory to a single unit cell, and obtained the frequency band structure as well as the wavenumber- (wave vector-) dependent damping ratio band structure.

Our results show that damping in general alters the shape of the frequency band structure. For the specific case of proportional damping, we observed from the discrete model results that the optical branch is more sensitive to stiffness-proportional damping, while the acoustical branch responds more readily to mass-proportional damping. The band gap shrinks or widens accordingly. These alterations induce both quantitative and qualitative changes to the group velocity dispersion curves. A significant consequence is the possibility of transition of

the group velocity corresponding to some branches from positive to negative as a result of damping [18].

Our results also revealed that when the damping is significant it could lead to rather dramatic changes to the frequency band structure (and hence the band gaps). In particular, we observed the branch overtaking phenomenon whereby the higher branches drop at a faster rate than the lower branches, thus allowing for the possibility of a branch overtake. We also observed, in the context of general damping, the phenomenon of a wavenumber (wave vector) band gap whereby in the case considered the acoustical branch experiences a cut-off, that is, it no longer spans the entire first Brillouin zone.

The treatment of damping using modal analysis and state-space transformation is common in the study of the *dynamics of structures* [19–21]. In this paper, and building on our earlier work [17, 18] we have extended the application of these techniques to the study of the *dynamics of materials* within the framework of Bloch theory. Incorporation of damping in this context is necessary as the newly emerging field of phononics – the science of phonons and their manipulation for technological applications – expands to incorporate a broader range of constituent material phases exhibiting different levels of dissipation. Since our formalisms revolve around the use of the damping matrix \mathbf{C} , we can fully utilize already

established quantitative models of damping in the finite structural dynamics literature [19–21]. Furthermore, the

presented formalisms are relevant to the study of Bloch wave propagation in other types of dissipative periodic media such as lossy photonic crystals [25–27].

-
- [1] M. S. Kushwaha, P. Halevi, L. Dobrzynski, and B. Djafari-Rouhani, “Acoustic band structure of periodic elastic composites,” *Physical Review Letters*, vol. 71, pp. 2022–2025, September 1993.
- [2] M. M. Sigalas, M. S. Kushwaha, E. N. Economou, M. Kafesaki, I. E. Psarobas, and W. Steurer, “Classical vibration modes in phononic lattices: theory and experiment,” *Zeitschrift für Kristallographie*, vol. 220, pp. 765–809, September 2005.
- [3] R. H. Olsson, III and I. El-Kady, “Microfabricated phononic crystal devices and applications,” *Measurement Science & Technology*, vol. 20, p. 012002, January 2009.
- [4] F. Bloch, “Über die quantenmechanik der elektronen in kristallgittern,” *Zeitschrift für Physik*, vol. 52, pp. 555–600, August 1929.
- [5] D. J. Mead, “A general theory of harmonic wave propagation in linear periodic systems with multiple coupling,” *Journal of Sound and Vibration*, vol. 27, pp. 235–260, March 1973.
- [6] S. Mukherjee and E. H. Lee, “Dispersion relations and mode shapes for waves in laminated viscoelastic composites by finite difference methods,” *Computers & Structures*, vol. 5, pp. 279–285, December 1975.
- [7] E. Tassilly, “Propagation of bending waves in a periodic beam,” *International Journal of Engineering Science*, vol. 25, pp. 85–94, 1987.
- [8] Y. Yong and Y. K. Lin, “Propagation of decaying waves in periodic and piecewise periodic structures of finite length,” *Journal of Sound and Vibration*, vol. 129, pp. 99–118, February 1989.
- [9] I. E. Psarobas, “Viscoelastic response of sonic band-gap materials,” *Physical Review B*, vol. 64, p. 012303, June 2001.
- [10] P. W. Mauriz, M. S. Vasconcelos, and E. L. Albuquerque, “Acoustic phonon power spectra in a periodic superlattice,” *Physica Status Solidi B*, vol. 243, pp. 1205–1211, March 2006.
- [11] R. Sprik and G. H. Wegdam, “Acoustic band gaps in composites of solids and viscous liquids,” *Solid State Communications*, vol. 106, pp. 77–81, April 1998.
- [12] X. Zhang, Z. Liu, J. Mei, and Y. Liu, “Acoustic band gaps for a two-dimensional periodic array of solid cylinders in viscous liquid,” *Journal of Physics: Condensed Matter*, vol. 15, pp. 8207–8212, November 2003.
- [13] Y. Liu, D. Yu, H. Zhao, J. Wen, and X. Wen, “Theoretical study of two-dimensional phononic crystals with viscoelasticity based on fractional derivative models,” *Journal of Physics D: Applied Physics*, vol. 41, p. 065503, February 2008.
- [14] W. Wang, J. Yu, and Z. Tang, “General dispersion and dissipation relations in a one-dimensional viscoelastic lattice,” *Physics Letters A*, vol. 373, pp. 5–8, December 2008.
- [15] B. Merheb, P. A. Deymier, M. Jain, M. Aleshyn-Lesuffleur, S. Mohanty, A. Berker, and R. W. Greger, “Elastic and viscoelastic effects in rubber/air acoustic band gap structures: A theoretical and experimental study,” *Journal of Applied Physics*, vol. 104, p. 064913, September 2008.
- [16] C.-Y. Lee, M. J. Leamy, and J. H. Nadler, “Frequency band structure and absorption predictions for multi-periodic acoustic composites,” *Journal of Sound and Vibration*, vol. 329, pp. 1809–1822, May 2010.
- [17] M. I. Hussein, “Reduced Bloch mode expansion for periodic media band structure calculations,” *Proceedings of the Royal Society A*, vol. 465, pp. 2825–2848, September 2009.
- [18] M. I. Hussein, “Theory of damped Bloch waves in elastic media,” *Physical Review B*, vol. 80, p. 212301, December 2009.
- [19] L. Meirovitch, *Principles and Techniques of Vibrations*. Prentice Hall, 1997.
- [20] J. Craig, Roy R. and A. J. Kurdila, *Fundamentals of Structural Dynamics*. John Wiley, 2nd ed., 2006.
- [21] T. K. Caughey and M. E. J. O’Kelly, “Classical normal modes in damped linear dynamic systems,” *Journal of Applied Mechanics Transactions of the ASME*, vol. 32, pp. 583–588, September 1965.
- [22] M. I. Hussein, K. Hamza, G. M. Hulbert, R. A. Scott, and K. Saitou, “Multiobjective evolutionary optimization of periodic layered materials for desired wave dispersion characteristics,” *Structural and Multidisciplinary Optimization*, vol. 31, pp. 60–75, January 2006.
- [23] M. I. Hussein, K. Hamza, G. M. Hulbert, and K. Saitou, “Optimal synthesis of 2D phononic crystals for broadband frequency isolation,” *Waves in Random and Complex Media*, vol. 17, pp. 491–510, October 2007.
- [24] M. I. Hussein, G. M. Hulbert, and R. A. Scott, “Dispersive elastodynamics of 1D banded materials and structures: design,” *Journal of Sound and Vibration*, vol. 307, pp. 865–893, November 2007.
- [25] V. Kuzmiak and A. A. Maradudin, “Distribution of electromagnetic field and group velocities in two-dimensional periodic systems with dissipative metallic components,” *Physical Review B*, vol. 58, pp. 7230–7251, September 1998.
- [26] C. Engström and M. Richter, “On the Spectrum of an Operator Pencil with Applications to Wave Propagation in Periodic and Frequency Dependent Materials,” *SIAM Journal on Applied Mathematics*, vol. 70, pp. 231–247, May 2009.
- [27] A. Raman and S. Fan, “Photonic band structure of dispersive metamaterials formulated as a Hermitian eigenvalue problem,” *Physical Review Letters*, vol. 104, p. 087401, February 2010.